Laser-Scanning Lithography (LSL) for the Soft Lithographic Patterning of Cell-Adhesive Self-Assembled Monolayers

Jordan S. Miller,[1] Mathilde I. Béthencourt,[2] Mariah Hahn,[1] T. Randall Lee,[2] Jennifer L. West[1]

[1]Department of Bioengineering, Rice University, P.O. Box 1892, MS-142, Houston, Texas 77251-1892; telephone: (713) 348-5955; fax: 713-348-5877; e-mail: jwest@rice.edu.
[2]Department of Chemistry, University of Houston, 4800 Calhoun Road, Houston, TX 77204-5003; telephone: (713) 743-2724; fax: 281-754-4445; e-mail: trlee@uh.edu

Received 19 August 2005; accepted 21 November 2005

Published online 27 January 2006 in Wiley InterScience (www.interscience.wiley.com). DOI: 10.1002/bit.20809

Abstract: We report the development of laser-scanning lithography (LSL), which employs a laser-scanning confocal microscope to pattern photoresists that can be utilized, for example, in the fabrication of masters for use in soft lithography. This convenient technique provides even exposure across the entire view field and facilitates accurate alignment of successive photoresist exposures. Features on the scale of 3 μm have been achieved to date with a 10× objective (NA 0.45). Virtual masks, instructions for laser irradiation, were drawn using the Region of Interest (ROI) function of a Zeiss LSM 510 microscope. These regions were then exposed to a 458 nm argon laser for 32 μs (0.9 mW/μm^2). Differential interference contrast (DIC) imaging was utilized with a non-destructive 514 nm argon laser as an immediate quality check of each exposure, to align successive exposures, and to reduce chromatic aberration between imaging and exposure. Developed masters were replica-molded with poly(dimethylsiloxane) (PDMS); these masters were then utilized for microcontact printing of cell-adhesive self-assembled monolayers (SAMs) to demonstrate the utility of this process. Initial studies confirmed that human dermal fibroblast adhesion and spreading were limited to cell-adhesive SAM areas. LSL is a rapid, flexible, and readily available technique that will accelerate master design and preparation; moreover, it can be applied to additional forms of photolithography and photopolymerization for studies in cell biology, biomaterials design and evaluation, materials science, and surface chemistry.

Keywords: cell adhesion; laser-ablation; peptide; photolithography; self assembly; cell patterning

INTRODUCTION

This work describes the development of laser-scanning lithography (LSL) to prepare micropatterned photoresist masters for use in lithographic applications. Photoresist masters have been utilized for replica-molding PDMS structures used in soft lithography (Chen et al., 1997; Jiang et al., 2005; Kane et al., 1999), microfluidics (Beebe et al., 2002; Jeon et al., 2000; Khademhosseini et al., 2004a), microelectronics (Yan et al., 2001), and biological applications, such as the construction of neuronal cell networks (Dertinger et al., 2002; Heller et al., 2005), the design of cellular arrays for high throughput screening (Chiu et al., 2000; Nelson et al., 2003), and other applications (Bhatia et al., 1997; Khademhosseini et al., 2004b; Suh et al., 2004). Indeed, several groups have been seeking to develop alternatives to traditional photolithography for the patterning of photoresists. Ideally, new methodologies should be highly flexible, widely available, and circumvent the need for a clean room. An inexpensive alternative has involved the adaptation of a fluorescent microscope for so-called microscope projection photolithography (MPP; Love et al., 2001). However, because a lamp is used as the light source, MPP inherently suffers from a Gaussian light intensity distribution across the entire view field. Uneven light intensity across the beam width means that optimal exposure settings at the center of the view field are different than those near the edge of the view field. Under- or over-exposure of the sample leads to pattern distortions, and therefore limits the total area of each view field that can be practically utilized. A more recent development has employed a liquid crystal display (LCD) projector as a programmable mask for projection photolithography (Itoga et al., 2004). A computer is connected to the LCD to project the computer screen image onto a given sample. However, this projection method leads to exposure artifacts from embedded electronic wires, which are necessary to control each pixel in the LCD.

Rather than whole area exposure, lithography in a serial fashion with a focused laser has been investigated (Ghislain et al., 1999; Rensch et al., 1989). The highly collimated light produced by the laser provides consistent exposure at the focal point. To create structures in more than one dimension, the sample is translated during exposure by the action of a

Correspondence to: T. Randall Lee; J.L. West
Contract grant sponsors: National Institutes of Health; National Science Foundation; National Aeronautics and Space Administration; Robert A. Welch Foundation

Contract grant numbers: RO1HL070537; ECS-0404308; NCC-1-02038; E-1320

This article includes Supplementary Material available via the Internet at http://www.interscience.wiley.com/jpages/0006-3592/suppmat.

programmable stage. Although this process is typically slower than whole area exposure due to the serial nature in which sample coordinates are addressed, the laser power and focal point position in the sample can be precisely controlled. Unfortunately, however, the extensive time required for the construction and optimization of these systems have limited their widespread use. Additionally, the necessity to translate the stage during exposure artificially limits the speed at which a given area can be addressed, compared to translating the laser beam across a fixed sample. Finally, these systems have been built to utilize only a single laser source, limiting their flexibility and the range of substrates that can be exposed.

In this work, we sought to utilize a commercially available laser-scanning confocal microscope as a readily available and highly flexible system for laser-scanning lithography (LSL). Confocal microscopes operate by focusing a laser of a given wavelength to a diffraction-limited size at the focal plane. The focal point can then be raster-scanned across the sample. The ability to control precisely the laser irradiation eliminates the need for traditional physical photomasks. In addition, the sample stage need not be translated during each exposure cycle because commercially available confocal microscopes—optimized over the past decade by several companies—now have raster scanning mirrors behind the objective. These mirrors enable the microscope to address up to 1 mm^2 or greater at a much faster rate and with fewer translational artifacts than if the sample stage were translated across a fixed beam. Confocal microscopes also have multiple aligned lasers that can be turned on and off independently for more complicated addressing of the sample (e.g., one laser for imaging and another for patterning). Multiple aligned lasers could also be useful for direct patterning of photoactive monolayers (Dillmore et al., 2004; Ryan et al., 2004). As an initial demonstration of the capabilities of LSL, we have employed this new method to create photoresist masters, and we have used these masters in conjunction with soft lithography to create micropatterned cell-adhesive self-assembled monolayers (SAMs).

Defining a Virtual Mask

The area of each view field of the microscope is determined by the properties of its optics and the objective chosen. A typical value for the view field area with a 10× objective (NA 0.45) is 922 × 922 μm. The computer controlling the microscope defines this area as an array of pixels, typically 2,048 × 2,048 pixels, which are sequentially addressed by the raster-scanning laser. Thus, in addition to the laser power (in these studies, 0.9 mW/μm^2), a critical parameter to define with LSL is the ''pixel time,'' or the residence time of the laser at each pixel location. Additionally, the number of ''iterations,'' or the total number of times the entire view field is scanned, can be defined.

Rather than conventional photomasks, LSL employs ''virtual masks'' to achieve addressable irradiation. These masks are simply bitmap images drawn onscreen that are converted into irradiation instructions, dictating at which pixel locations the shutter of the laser is open or closed during each raster-scanning cycle. To create these bitmap images, the user simply draws shapes onscreen to be exposed. The true dimensions of each drawn object, in μm, can be easily calculated once the pixel to μm conversion factor is known (~2.2 pixels/μm along both the x- and y-axis, based on the above values). The types of shapes that can currently be drawn using the microscope software include rectangles, ellipses, closed Bezier curves, and polygons. After drawing is complete, the computer converts all drawn shapes into programming instructions for the shutter of the laser (Fig. 1). In this manner, LSL allows for addressable irradiation without the need for a conventional physical photomask.

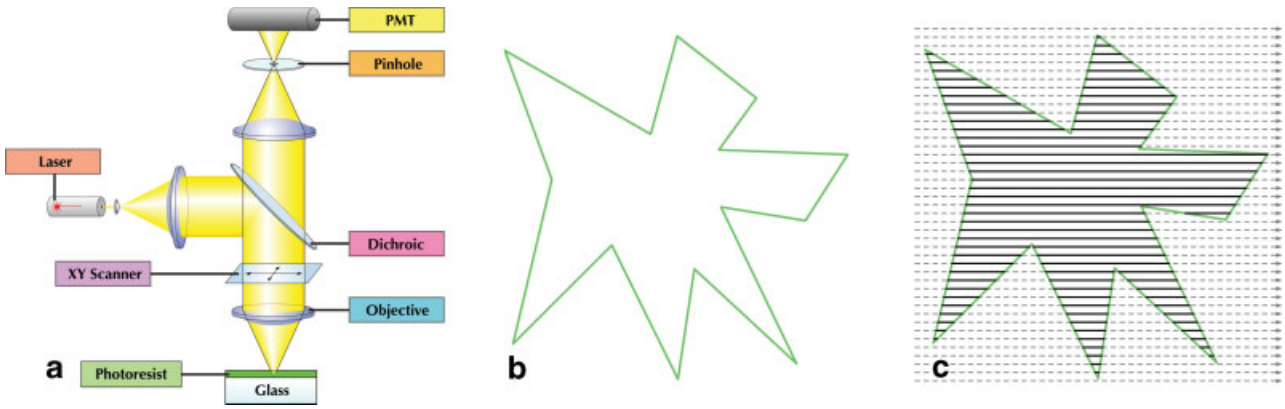

Figure 1. Schematic of laser-scanning lithography (LSL). **a**: LSL utilizes a laser-scanning confocal microscope for addressable irradiation of a photosensitive material, such as photoresist. Programmatic control of the xy-scanner and laser shutter enables addressable irradiation without the need for a physical photomask (adapted with permission from Carl Zeiss, Inc.). **b**: A bitmap image is drawn onscreen using tools available in the software of the microscope, and serves as a virtual mask. **c**: The computer converts the virtual mask into irradiation instructions for exposure. The focal point of the microscope is unidirectionally raster scanned across the view field with the laser shutter closed (dashed arrows). When the scanning focal point intersects a pixel inside the virtual mask, the laser shutter is opened for the programmed pixel time (solid lines).

Biotechnology and Bioengineering. DOI 10.1002/bit

MATERIALS AND METHODS

Hexamethyldisilazane (HMDS), 16-mercaptohexadecanoic acid, 3-mercaptopropyltrimethoxysilane, hexaethylene glycol, *N*-hydroxybenzotriazole (HOBt), and *N*-(3-dimethylaminopropyl)-*N*′-ethylcarbodiimide (EDC) were purchased from Sigma-Aldrich (St. Louis, MO) and used as received, unless otherwise specified. Gold shot (>99.99%) was purchased from Americana Precious Metals (East Rutherford, NJ). The solvents dichloromethane (DCM), tetrahydrofuran (THF), dimethylformamide (DMF), methanol (MeOH), and ethyl acetate (EtOAc) were purchased from EMD Chemicals (Gibbstown, NJ) and used as received, unless noted otherwise.

Preparation of Gold-Coated Coverslips

Round coverslips (22 mm; Fisher Scientific, Pittsburgh, PA) were cleaned with ''piranha solution'' (7:3 concentrated H_2SO_4/30% H_2O_2) and then rinsed with deionized water. *Caution: piranha solution reacts violently with organic materials and should be handled carefully.* The coverslips were next treated with a mixture of H_2O_2, NH_4OH, and H_2O (1:1:5) at 80°C for 1 h, and then rinsed with deionized water. The glass surface was functionalized with 3-mercaptopropyltrimethoxysilane by immersion at 80°C for 1 h in a mixture of water and isopropyl alcohol (1:4) containing the silane. The coverslips were then rinsed with isopropyl alcohol, blown dry with nitrogen, and dried at 100°C for 10 min. Thermal evaporation of gold yielded a 100 Å gold layer on these coverslips.

Preparation of Photoresist-Coated Coverslips

Premium #1 coverslips (Fisher Scientific) were primed with HMDS for 10 s and spun dry. Microposit S1813 photoresist (Shipley, Marlborough, MA) was spin coated to a thickness of 1.3 μm (4,000 rpm for 40 s) and soft-baked in an oven at 100°C for 5 min.

Laser-Scanning Lithography

A Zeiss LSM 510 microscope (Carl Zeiss, Oberkochen, Germany) and its accompanying LSM 5 software were used for LSL. To define a virtual mask, shapes were drawn using the ''Region of Interest'' (ROI) function of the LSM 5 software. Exposures were performed with a 458 nm argon laser at a pixel to μm conversion factor of 4.93 pixels^2/μm^2 (2,048 × 2,048 pixels = 922 × 922 μm), an exposure intensity of 0.9 mW/μm^2, and a pixel time of 6.4 μs (32 μs/μm^2). Differential interference contrast (DIC) imaging was performed with a non-destructive 514 nm argon laser.

Replica-Molding of PDMS

Photoresist masters prepared by LSL were coated with (tridecafluoro-1,1,2,2-tetrahydrooctyl)-1-trichlorosilane (United Chemical Technologies, Bristol, PA) by vacuum deposition in a dessicator for 1 h at 100°C. After cooling, a PDMS prepolymer (Sylgard 184, Dow Corning, Midland, MI) was poured onto the photoresist and cured at 150°C for 15 min. The resulting PDMS stamps were removed by hand.

Soft Lithography

To create a binary surface of self-assembled monolayers (SAMs), functionalized thioalkanes were synthesized. A thioalkane terminated with an oligoethylene glycol (OEG) moiety (thioalkane-OEG, **1**) was prepared according to Figure 2 and the following paragraphs. This type of alkanethiol has been shown to have cell non-adhesive properties (Jiang et al., 2004; Prime and Whitesides, 1991).

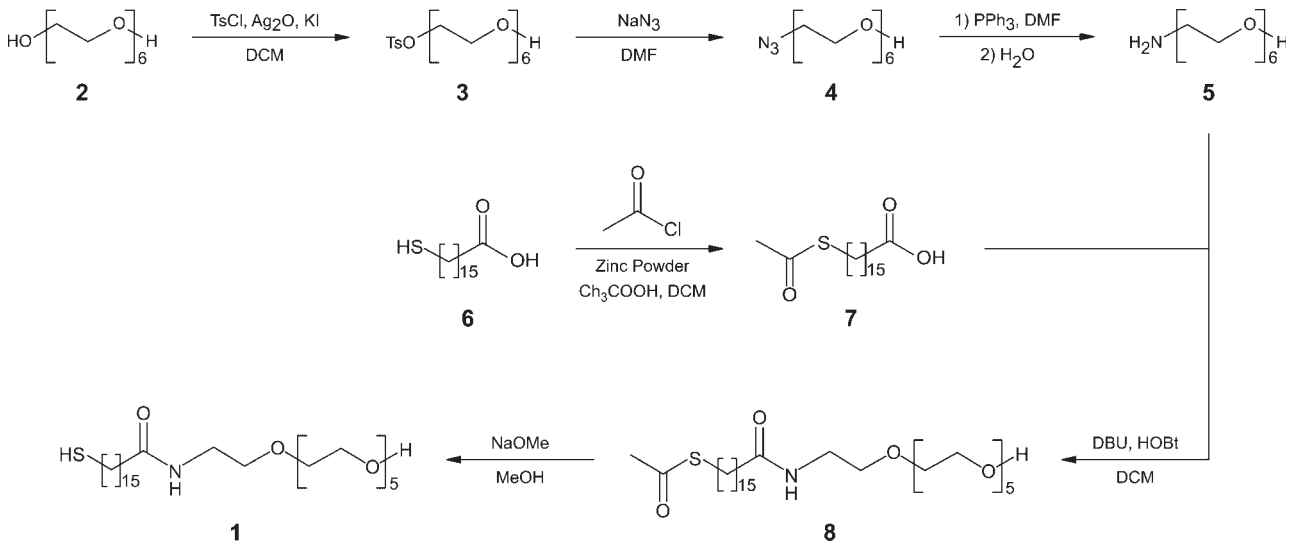

Figure 2. Synthesis of thioalkane-OEG.

DOI 10.1002/bit

Convenient methods to monosubstitute hexaethylene glycol with a primary amine were performed as previously described (Loiseau et al., 2004; Svedhem et al., 2001). The intermediates and products were characterized by NMR spectroscopy in $CDCl_3$ using a QE-300 spectrometer (300 MHz ^1H).

Synthesis of $HO(CH_2CH_2O)_5CH_2CH_2OTs$ (3)

To a chilled and stirred solution of hexaethylene glycol (**2**) (5.0 g, 18 mmol) in DCM were added: Ag_2O (6.2 g, 27 mmol), TsCl (3.7 g, 20 mmol), and KI (0.6 g, 4 mmol). After stirring for 1 h, the precipitated silver salts were removed by filtration through celite. The celite cake was thoroughly washed with EtOAc. The combined filtrates were evaporated, and the residue was purified by column chromatography (2% MeOH in DCM) to afford pure **3** in 79% yield. ^1H NMR: δ 7.79 (d, $J = 6.6$ Hz, 2 H), 7.33 (d, $J = 8.4$ Hz, 2 H), 4.15 (t, $J = 5.7$ Hz, 2 H), 3.47–3.71 (m, 22 H), 2.45 (s, 3 H).

Synthesis of $HO(CH_2CH_2O)_5CH_2CH_2N_3$ (4)

To a solution of **3** (2.5 g, 5.7 mmol) in DMF, sodium azide (0.6 g, 9 mmol) was added. The stirred mixture was warmed to 110°C. After 2.5 h, the solution was cooled to room temperature, and the DMF was removed by distillation. The residue was purified by column chromatography (5% MeOH in DCM) to afford pure **4** in 99% yield. ^1H NMR: δ 3.59–3.71 (m, 22 H), 3.39 (t, $J = 5.4$ Hz, 2 H).

Synthesis of $HO(CH_2CH_2O)_5CH_2CH_2NH_2$ (5)

To a chilled solution (0°C) of **4** (1.8 g, 5.9 mmol) in dry THF (previously distilled from $LiAlH_4$), triphenylphosphine (1.7 g, 6.5 mmol) was added. The solution was stirred for 10 h at room temperature. Water (1 mL) was then added, and the solution was stirred for an additional 3 h. The solvent was evaporated, and the residue was purified by column chromatography (MeOH:DCM:Et_3N, 3:3:1) to afford pure **5** in 76% yield. ^1H NMR: δ 3.73 (t, $J = 3.6$ Hz, 2 H), 3.58–3.67 (m, 18 H), 3.52 (t, $J = 5.1$ Hz, 2 H), 2.87 (t, $J = 5.7$ Hz, 2 H).

Synthesis of $AcS(CH_2)_{15}COOH$ (7)

To a solution of DCM (15 mL) and acetic acid (15 mL), 16-mercaptohexadecanoic acid (**6**) (1.5 g, 5.2 mmol) was dissolved. Zinc powder (3.0 g) was added, and the mixture was stirred for 1 h at room temperature. After cooling at 0°C, acetyl chloride was added (7.4 mL, 0.10 mol). When the production of hydrogen gas ceased, the reaction was brought to room temperature and stirred for an additional 30 min. The zinc powder was then removed by filtration through celite, and the organic filtrate was washed twice with 0.1M HCl. The solution was dried over anhydrous magnesium sulfate, filtered, and evaporated. The residue was purified by column chromatography (EtOAc) to afford pure **7** in 89% yield. ^1H NMR: δ 2.86 (t, $J = 7.8$ Hz, 2 H), 2.36 (t, $J = 7.2$ Hz, 2 H), 2.34 (s, 3 H), 1.64 (m, 2 H), 1.54 (m, 2 H), 1.25 (bs, 22 H).

Synthesis of $AcS(CH_2)_{15}CONHCH_2CH_2(OCH_2CH_2)_5OH$ (8)

To a solution of dried DCM (30 mL), $AcS(CH_2)_{15}COOH$ (**7**) (1.6 g, 4.7 mmol) was dissolved, and the solution was cooled to 0°C. $HO(CH_2CH_2O)_5CH_2CH_2NH_2$ (**5**; 2.0 g, 7.1 mmol) was added, as well as *N*-hydroxybenzotriazole (HOBt, 1.0 g, 7.1 mmol), and *N*-(3-dimethylaminopropyl)-*N*′-ethylcarbodiimide (EDC, 1.4 g, 7.1 mmol). The reaction mixture was warmed to room temperature and stirred for 12 h. The mixture was then diluted with DCM, and washed first with 0.1M HCl and then with water. The solution was dried over anhydrous magnesium sulfate, filtered, and evaporated. The residue was purified by column chromatography (3% MeOH in DCM) to afford pure **8** in 75% yield. ^1H NMR: δ 3.73 (t, $J = 4.2$ Hz, 2 H), 3.66 (bm, 18 H), 3.55 (t, $J = 4.8$ Hz, 2 H), 3.44 (t, $J = 4.8$ Hz, 2 H), 2.87 (t, $J = 7.5$ Hz, 2 H), 2.33 (s, 3 H), 2.19 (t, $J = 7.5$ Hz, 2 H), 1.57 (m, 4 H), 1.24 (bs, 22 H).

Synthesis of $HS(CH_2)_{15}CONHCH_2CH_2(OCH_2CH_2)_5OH$ (1)

To a solution of methanol, $AcS(CH_2)_{15}CONHCH_2$-$CH_2(OCH_2CH_2)_5OH$ (**8**) (1.7 g, 2.9 mmol) was dissolved, and the flask was purged with argon. Sodium methoxide (0.5M in methanol, 29 mL, 14 mmol) was added to the solution, and the mixture was stirred for 1 h. The reaction was then neutralized with Dowex H^+ resin, and the solvent was evaporated. The residue was purified by column chromatography (3% MeOH in DCM) to afford pure **1** in 96% yield. ^1H NMR: δ 3.72 (t, $J = 5.7$ Hz, 2 H), 3.66 (bm, 18 H), 3.56 (t, $J = 4.8$ Hz, 2 H), 3.44 (t, $J = 5.1$ Hz, 2 H), 2.51 (q, $J = 7.8$ Hz, 2 H), 2.18 (t, $J = 7.5$ Hz, 2 H), 1.59 (m, 4 H), 1.24 (bs, 22 H).

Synthesis of Thioalkane-OEG-GRGDS (9)

Thioalkane-OEG-GRGDS was efficiently synthesized using Fmoc solid-phase peptide synthesis (431A Synthesizer, Applied Biosystems, Foster City, CA) according to Figure 3 (a similar scheme has been previously described, see Houseman and Mrksich, 1998). Following chain extension of the GRGDS peptide on the resin, the commercially available *O*-(*N*-Fmoc-2-aminoethyl)-*O*′-(2-carboxyethyl)-undecaethyleneglycol (**10**, Novabiochem, UK), and then (16-tritylsulfanyl)hexadecanoic acid (**11**), were incorporated. Cleavage from the resin was effected with 95% TFA, 2.5% H_2O, 2.5% triisopropylsilane (TIPS; Pearson et al., 1989) to give thioalkane-OEG-GRGDS (**9**). This thioalkane is connected to an OEG spacer and terminated with the cell-adhesive GRGDS sequence to give a molecule that forms a cell-adhesive SAM (Houseman and Mrksich, 1998; Roberts et al., 1998). Note that although the GRGDS sequence was chosen for these studies, the strategy shown in Figure 3 can be

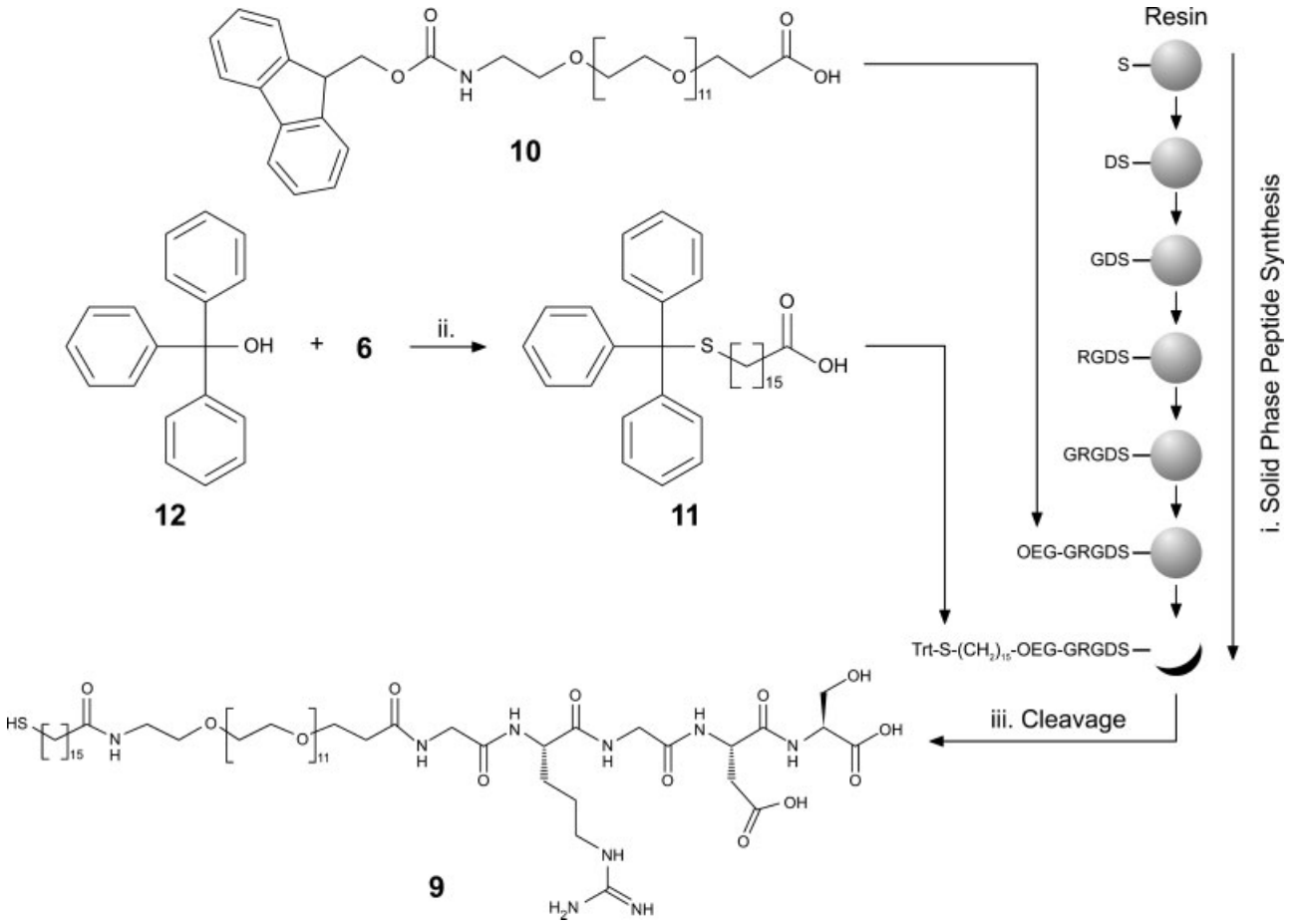

Figure 3. Synthesis of thioalkane-OEG-GRGDS by solid-phase peptide synthesis (SPPS). (i) Solid-phase peptide synthesis (SPPS) via the Fmoc strategy, (ii) neat TFA; evaporation; diethyl ether extraction, (iii) 95% TFA, 2.5% H_2O, 2.5% TIPS.

utilized for the efficient synthesis of any peptide-terminated alkanethiol of interest.

Synthesis of (16-Tritylsulfanyl)Hexadecanoic Acid (11)

The trityl protection of **6** was effected with triphenylmethanol (**12**) and TFA as previously described for the trityl protection of cysteine (Photaki et al., 1970). A 1:1.2 mixture of **6** (2.70 g, 9.37 mmol) and **12** (2.93 g, 11.2 mmol) was dissolved in neat TFA (18 mL) and stirred at room temperature for 1 h. The TFA was removed under vacuum. The crude mixture was dissolved in diethyl ether (20 mL) and sodium acetate (25% w/v in deionized H_2O, 50 mL), and extracted three times with diethyl ether (120 mL). The extracted organic phases were combined and evaporated, and the residue was purified by column chromatography (25% diethyl ether in hexanes) to afford pure **11**. ^{1}H NMR: δ 7.40 (m, 6 H), 7.20–7.30 (m, 9 H), 2.35 (t, $J = 7.2$ Hz, 2 H), 2.12 (t, $J = 7.5$ Hz, 2 H), 1.62 (m, 2 H), 1.26 (bs, 24 H).

Microcontact Printing

PDMS stamps were dipped in an ethanolic solution of **1** (2 mM) and dried under a stream of argon. Stamps were gently applied to gold-coated coverslips for 10–30 s. After removing the stamp, the slides were dipped in an ethanolic solution of **9** (2 mM) for 2 min to coat unmodified areas of the gold surface.

Cell Culture

Human dermal fibroblasts (HDFs, Cambrex, East Rutherford, NJ) were maintained in Dulbecco's modified Eagle medium containing 10% fetal bovine serum, 2 mM L-glutamine, 1,000 U/mL penicillin, and 100 mg/L streptomycin at 37°C/5% CO_2. Cells were used at passage 5–9, and seeded onto SAM-modified coverslips at a density of 3.1×10^5 cells/cm^2. Photographs were taken at 3 h, and the fidelity of the cell patterns were optically verified over the first 24 h.

RESULTS AND DISCUSSION

Identifying Optimal Parameters for LSL

To determine optimal exposure parameters for LSL, we performed several arrays of exposures for a given combination of positive photoresist (S1813), laser wavelength (458 nm), and microscope objective (10×, NA 0.45).

DOI 10.1002/bit

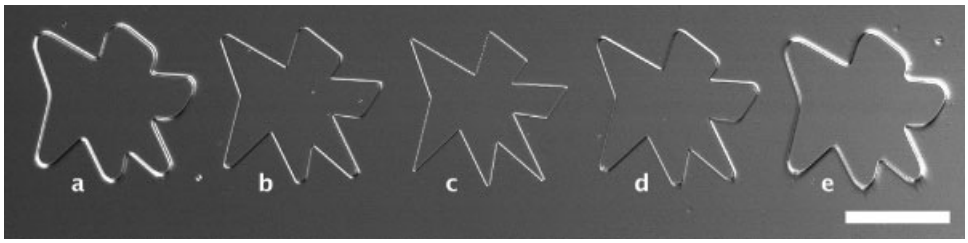

Figure 4. Dependence of fidelity on focus. Using the virtual mask from Figure 1b, the photoresist was exposed in or out of focus and then developed (z-position of focal point relative to photoresist: **a** = −40.0 μm, **b** = −20.0 μm, **c** = 0.0 μm [in focus], **d** = +20.0 μm, **e** = +40.0 μm; 1 scan, 6.4 μs pixel time, 0.9 mW/μm^2). Accurate focusing greatly influences the concordance of the exposed region with the original virtual mask. Scale bar = 100 μm.

Dependence of Fidelity on Focus

The width of the laser beam outside of the focal plane spreads by $2Z\lambda/\pi\omega_0$ where ω_0 is half the width of the laser beam at the focal plane, and Z is axial distance from the focal plane (Guenther, 1990). Thus, even when using a thin photoresist layer, positioning the photoresist tens of microns out of focus led to noticeably blurred features (Fig. 4).

Dependence of Fidelity on Laser Power

Power settings required for adequate exposure were assessed using an intermediate pixel time (6.4 μs) and a single iteration (Fig. 5). At low power levels, some feature definition was present, but there were considerable artifacts from the scanning laser. As the power level was increased, even exposure of the area was achieved while maintaining high lateral resolution. Higher power settings gave the smoothest exposures. An intermediate power setting of 0.9 mW/μm^2 was chosen as the optimal setting.

Dependence of Fidelity on Pixel Time and Iterations

Optimal pixel time settings were assessed using a fixed power setting (0.9 mW/μm^2) and a single iteration (Fig. 6). At long pixel residence times, the exposure was even but time-consuming (∼100 s to expose the virtual mask). Short pixel times completed the exposure faster but showed scanning artifacts. Even after compensating with high power, a short pixel time was unable to completely expose the photoresist. An intermediate pixel time of 6.4 μs (∼12 s to expose the virtual mask) was chosen as the optimal setting for maximum speed and fidelity.

The number of iterations required for optimal exposure was assessed using a fixed pixel time (0.64 μs) and laser power setting (0.9 mW/μm^2). Although scanning artifacts from this shortest pixel time could be compensated with multiple iterations, other inaccuracies arose (Fig. 7). The fidelity of the exposure depends on the shutter of the laser operating on a faster time scale than the scanning laser. Using a pixel time of 0.64 μs, the scanning speed surpassed the speed at which the shutter of the laser could operate, leading to elongation of the smallest features (highlighted in Fig. 7c). A high number of scans made potential registration issues apparent, and led to the widening of all exposed regions (up to ∼10% for 100 iterations). These results confirm that an intermediate pixel time of 6.4 μs and a single scan are needed to maximize efficiency while maintaining fidelity.

DIC Imaging for Focus and Alignment

Another advantage of LSL is that DIC imaging can be used for focusing on the photoresist and aligning successive exposures. A non-destructive 514 nm laser was used initially to image the photoresist and focus on the surface. Following exposure by LSL, the non-destructive laser was used to observe the exposed regions. DIC imaging provides contrast based on differences in indices of refraction within the sample. Exposing the photoresist photochemically changes these regions sufficiently to provide the contrast needed for visualization. The ability to observe exposed regions of undeveloped photoresist aided in the alignment of successive exposures. Manually translating the stage allowed for precise alignment of the next exposure (precision is approximately 3 μm). Development of the photoresist showed good agreement with the area seen with DIC imaging (Fig. 8). Additionally, because the imaging and exposing lasers were

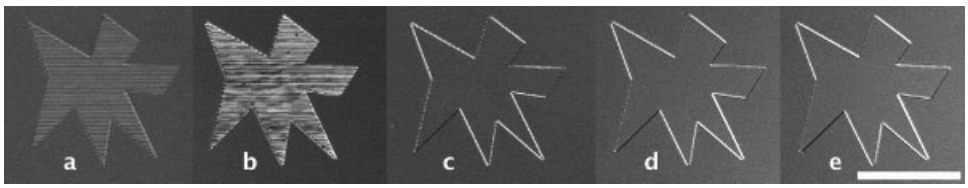

Figure 5. Dependence of even exposure on laser power. Using the virtual mask from Figure 1b, the photoresist was exposed to various laser power settings and then developed (**a** = 0.14 mW/μm^2, **b** = 0.24 mW/μm^2, **c** = 0.33 mW/μm^2, **d** = 0.9 mW/μm^2, **e** = 1.2 mW/μm^2; 1 scan, 6.4 μs pixel time). a, b: These low power levels gave poor exposure contrast and showed scanning artifacts. c: An intermediate power level began to show good exposure contrast and detail. d, e: These high power levels gave the smoothest exposures. Scale bar = 100 μm.

Biotechnology and Bioengineering. DOI 10.1002/bit

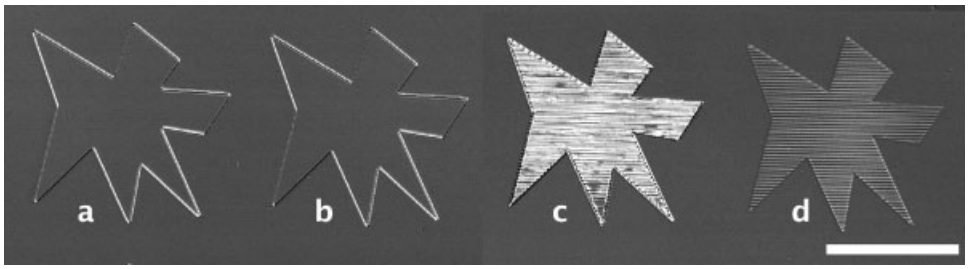

Figure 6. Dependence of fidelity on pixel time. Using the virtual mask from Figure 1b, the photoresist was exposed to various pixel time settings and then developed (**a** = 51.2 μs, **b** = 25.6 μs, **c** = 3.2 μs, **d** = 1.6 μs; 1 scan, 0.9 mW/μm^2). a, b: These long pixel times gave time-consuming but even exposures. c, d: Short pixel times gave faster exposures but required higher laser power to fully expose the photoresist. Failure to increase the laser power with decreasing pixel time led to scanning artifacts. Scale bar = 100 μm.

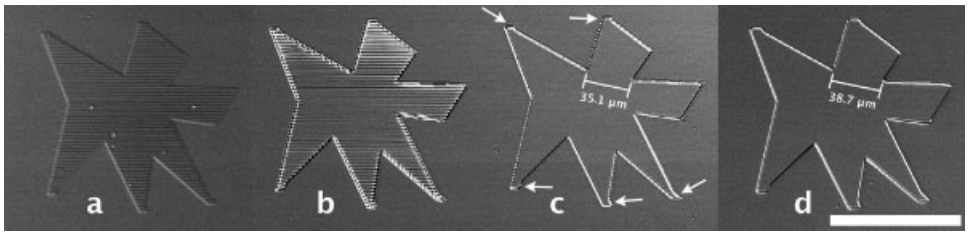

Figure 7. Dependence of fidelity on number of iterations. Using the virtual mask from Figure 1b, the photoresist was exposed to various iterations and then developed (**a** = 8 scans, **b** = 16 scans, **c** = 20 scans, **d** = 100 scans; 0.64 μs pixel time, 0.9 mW/μm^2). Scanning artifacts (a, b) were compensated with increased iterations, to smooth the exposure (c). However, short pixel times (i.e., 0.64 μs) led to distortions of narrow features, as the scanning speed surpassed the speed at which the shutter of the laser could operate. These distortions were manifested as elongations along the direction of scanning (compare the arrows in c with the virtual mask in Figure 1b). d: A high number of scans led to decreased fidelity due to widening of the exposed area (measured distance in c = 35.1 μm, d = 38.7 μm). The microscope was unable to keep accurate registration during a high number of rapid scans. Scale bar = 100 μm.

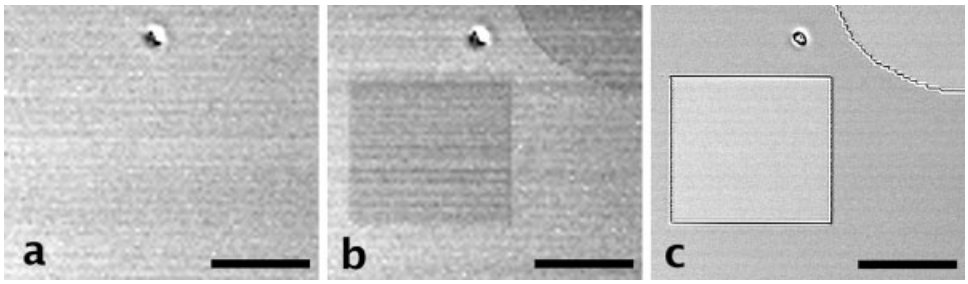

Figure 8. Another advantage of LSL is the ability to observe exposed regions of photoresist with DIC imaging before developing. **a**: Unexposed photoresist was imaged with a non-destructive 514 nm argon laser to locate the surface. **b**: Following LSL with a 458 nm argon laser, the 514 nm laser was again used to image the exposed regions. **c**: Confirmation that the regions of increased contrast were exposed during LSL is seen in the developed photoresist. Scale bar = 50 μm.

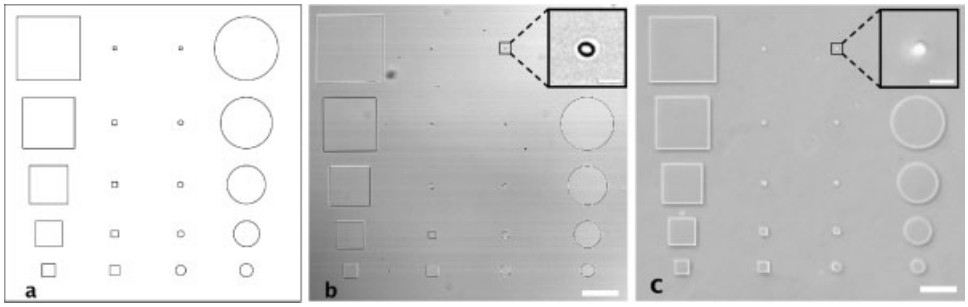

Figure 9. Replica-molding of poly(dimethylsiloxane) (PDMS) from a photoresist master created with LSL. **a**: Virtual mask drawn onscreen, (**b**) developed photoresist master, and (**c**) replica molded PDMS. Scale bar = 100 μm. The minimum feature size achieved with a 10× objective (NA 0.45) was 3 μm (enlarged in b, c; scale bar = 5 μm).

DOI 10.1002/bit

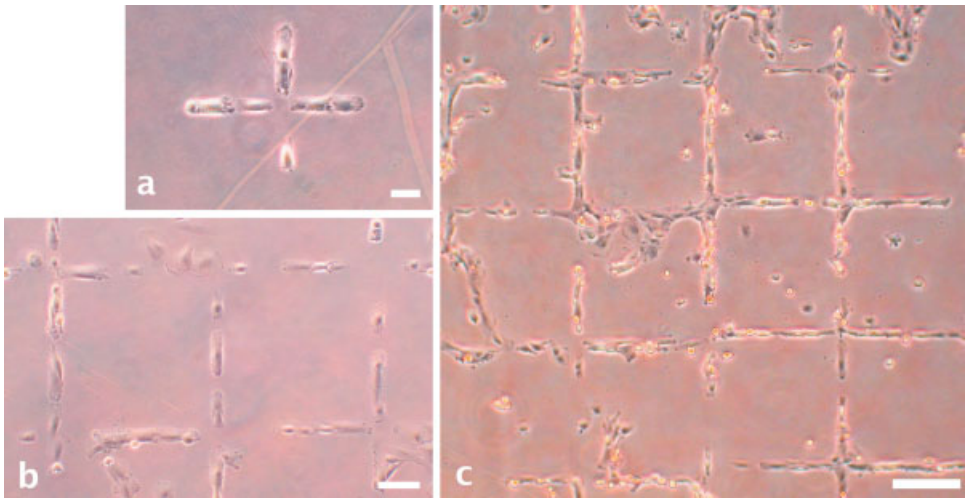

Figure 10. Cell patterns created by soft lithography. Non-adhesive 360 μm squares were stamped with thioalkane-OEG on a gold-coated surface (Prime and Whitesides, 1991). Intervening 10 μm lines were then backfilled with the adhesive thioalkane-OEG-GRGDS (Roberts et al., 1998). Human dermal fibroblasts were cultured on these surfaces and photographed with phase contrast microscopy. Scale bars: **a** = 50 μm, **b** = 100 μm, **c** = 200 μm.

similar in wavelength, chromatic aberration that can result from focusing with visible light (450–750 nm) and exposing with UV light (300–450 nm) was greatly reduced.

LSL Masters for Soft Lithography

To demonstrate the utility of LSL, soft lithography was performed with masters generated by LSL. Photoresist masters prepared with a 10× objective were replica-molded into PDMS. Features with 3 μm resolution could be fabricated with high reproducibility (Fig. 9). Binary surfaces of self-assembled monolayers (SAMs) were created on gold-coated substrates by microcontact printing of functionalized alkanethiols with these micromolded PDMS stamps (Chen et al., 1997; Jiang et al., 2005; Kane et al., 1999). Regions were formed that inhibited or promoted mammalian cell attachment by using thioalkane-OEG (OEG = oligoethylene glycol) or thioalkane-OEG-GRGDS (GRGDS = Gly-Arg-Gly-Asp-Ser peptide sequence), respectively (Prime and Whitesides, 1991; Roberts et al., 1998; Fig. 10). The small defects present in the cell patterns are believed to reflect the high surface packing density of the thioalkane-OEG used. Adding a small percentage of CH_3-terminated thioalkane would afford a lower surface packing density of this SAM and should decrease cell pattern defects (Li et al., 2005).

CONCLUSIONS

Laser-scanning lithography of photoresist masters enables micron-scale features to be generated with high fidelity and greater facility than conventional photomasking. Various parameters can be precisely controlled by the user to allow maximum flexibility, such as the laser power, the pixel time, and the number of iterations. DIC imaging permits immediate verification of each exposure, precise alignment of successive scans, and reduced chromatic aberration between imaging and exposure. LSL rapidly produces masters for use in soft lithography, and its utility was verified by HDF confinement within micropatterned SAMs. A current limitation of this technique is that maximum fidelity can be achieved only with thin photoresist layers due to the width of the laser beam outside of the focal plane. Future studies will characterize the minimum feature size possible with this method. The minimum lateral feature size possible should be, in practice, approximately the wavelength of light used (∼500 nm or smaller) due to diffractional limitations (Love et al., 2001). The maximum feature size possible in the axial direction can be expanded through cycles of photoresist deposition and exposure, or by multiphoton irradiation. Multiphoton or two-photon photopolymerization will be a particularly useful modification of this system as the buildup of arbitrary three-dimensional structures should be possible without the need for layer-by-layer substrate deposition. Additionally, multiphoton photopolymerization could allow even smaller features (e.g., at or below 1 micron) to be readily obtained (Cumpston et al., 1999). LSL is applicable to other forms of microfabrication, such as SU-8 negative photoresist photolithography or PEG hydrogel photopolymerization (Hahn et al., 2005), which are areas under current investigation. We believe the equipment required for LSL is readily available at many institutions, and that many scientific disciplines will find this technique advantageous when compared to conventional photomasking.

We thank Prof. Rebekah Drezek for helpful discussions.

References

Beebe DJ, Mensing GA, Walker GM. 2002. Physics and applications of microfluidics in biology. Annu Rev Biomed Eng 4:261–286.

Bhatia SN, Yarmush ML, Toner M. 1997. Controlling cell interactions by micropatterning in co-cultures: Hepatocytes and 3T3 fibroblasts. J Biomed Mater Res 34(2):189–199.

Chen CS, Mrksich M, Huang S, Whitesides GM, Ingber DE. 1997. Geometric control of cell life and death. Science 276(5317):1425–1428.

Chiu DT, Jeon NL, Huang S, Kane RS, Wargo CJ, Choi IS, Ingber DE, Whitesides GM. 2000. Patterned deposition of cells and proteins onto surfaces by using three-dimensional microfluidic systems. Proc Natl Acad Sci USA 97(6):2408–2413.

Cumpston BH, Ananthavel SP, Barlow S, Dyer DL, Ehrlich JE, Erskine LL, Heikal AA, Kuebler SM, Lee IYS, McCord-Maughon D, Quin J, Röckel H, Rumi M, Wu X, Marder SR, Perry JW. 1999. Two-photon polymerization initiators for three-dimensional optical data storage and microfabrication. Nature 398(6722):51–54.

Dertinger SK, Jiang X, Li Z, Murthy VN, Whitesides GM. 2002. Gradients of substrate-bound laminin orient axonal specification of neurons. Proc Natl Acad Sci USA 99(20):12542–12547.

Dillmore WS, Yousaf MN, Mrksich M. 2004. A photochemical method for patterning the immobilization of ligands and cells to self-assembled monolayers. Langmuir 20(17):7223–7231.

Ghislain LP, Elings VB, Crozier KB, Manalis SR, Minne SC, Wilder K, Kino GS, Quate CF. 1999. Near-field photolithography with a solid immersion lens. Appl Phys Lett 74(4):501–503.

Guenther RD. 1990. Modern optics. New York: John Wiley & Sons. 720p.

Hahn MS, Miller JS, West JL. 2005. Laser scanning lithography for surface micropatterning on hydrogels. Adv Mater (in press).

Heller DA, Garga V, Kelleher KJ, Lee TC, Mahbubani S, Sigworth LA, Lee TR, Rea MA. 2005. Patterned networks of mouse hippocampal neurons on peptide-coated gold surfaces. Biomaterials 26(8):883–889.

Houseman BT, Mrksich M. 1998. Efficient solid-phase synthesis of peptide-substituted alkanethiols for the preparation of substrates that support the adhesion of cells. J Org Chem 63(21):7552–7555.

Itoga K, Yamato M, Kobayashi J, Kikuchi A, Okano T. 2004. Cell micropatterning using photopolymerization with a liquid crystal device commercial projector. Biomaterials 25(11):2047–2053.

Jeon NL, Dertinger SKW, Chiu DT, Choi IS, Stroock AD, Whitesides GM. 2000. Generation of solution and surface gradients using microfluidic systems. Langmuir 16(22):8311–8316.

Jiang X, Bruzewicz DA, Thant MM, Whitesides GM. 2004. Palladium as a substrate for self-assembled monolayers used in biotechnology. Anal Chem 76(20):6116–6121.

Jiang X, Bruzewicz DA, Wong AP, Piel M, Whitesides GM. 2005. Directing cell migration with asymmetric micropatterns. Proc Natl Acad Sci USA 102(4):975–978.

Kane RS, Takayama S, Ostuni E, Ingber DE, Whitesides GM. 1999. Patterning proteins and cells using soft lithography. Biomaterials 20(23–24):2363–2376.

Khademhosseini A, Suh KY, Jon S, Eng G, Yeh J, Chen GJ, Langer R. 2004a. A soft lithographic approach to fabricate patterned microfluidic channels. Anal Chem 76(13):3675–3681.

Khademhosseini A, Suh KY, Yang JM, Eng G, Yeh J, Levenberg S, Langer R. 2004b. Layer-by-layer deposition of hyaluronic acid and poly-L-lysine for patterned cell co-cultures. Biomaterials 25(17):3583–3592.

Li L, Chen S, Zheng J, Ratner BD, Jiang S. 2005. Protein adsorption on oligo(ethylene glycol)-terminated alkanethiolate self-assembled monolayers: The molecular basis for nonfouling behavior. J Phys Chem B 109(7):2934–2941.

Loiseau FA, Hii KKM, Hill AM. 2004. Multigram synthesis of well-defined extended bifunctional polyethylene glycol (PEG) chains. J Org Chem 69(3):639–647.

Love JC, Wolfe DB, Jacobs HO, Whitesides GM. 2001. Microscope projection photolithography for rapid prototyping of masters with micron-scale features for use in soft lithography. Langmuir 17(19): 6005–6012.

Nelson CM, Raghavan S, Tan JL, Chen CS. 2003. Degradation of micropatterned surfaces by cell-dependent and -independent processes. Langmuir 19(5):1493–1499.

Pearson DA, Blanchette M, Baker ML, Guindon CA. 1989. Trialkylsilanes as scavengers for the trifluoroacetic acid deblocking of protecting groups in peptide synthesis. Tetrahedron Lett 30(21):2739–2742.

Photaki I, Taylor-Papadimitriou J, Sakarellos C, Mazarakis P, Zervas L. 1970. On cysteine and cystine peptides. Part V. S-trityl- and S-diphenyl-methyl-cysteine and -cysteine peptides. J Chem Soc C 19:2683–2687.

Prime KL, Whitesides GM. 1991. Self-assembled organic monolayers: model systems for studying adsorption of proteins at surfaces. Science 252(5010):1164–1167.

Rensch C, Hell S, Vonschickfus M, Hunklinger S. 1989. Laser scanner for direct writing lithography. Appl Optics 28(17):3754–3758.

Roberts C, Chen CS, Mrksich M, Martichonok V, Ingber DE, Whitesides GM. 1998. Using mixed self-assembled monolayers presenting RGD and (EG)(3)OH groups to characterize long-term attachment of bovine capillary endothelial cells to surfaces. J Am Chem Soc 120(26):6548–6555.

Ryan D, Parviz BA, Linder V, Semetey V, Sia SK, Su J, Mrksich M, Whitesides GM. 2004. Patterning multiple aligned self-assembled monolayers using light. Langmuir 20(21):9080–9088.

Suh KY, Seong J, Khademhosseini A, Laibinis PE, Langer R. 2004. A simple soft lithographic route to fabrication of poly(ethylene glycol) microstructures for protein and cell patterning. Biomaterials 25(3): 557–563.

Svedhem S, Hollander CA, Shi J, Konradsson P, Liedberg B, Svensson SCT. 2001. Synthesis of a series of oligo(ethylene glycol)-terminated alkanethiol amides designed to address structure and stability of biosensing interfaces. J Org Chem 66(13):4494–4503.

Yan M, Koide Y, Babcock JR, Markworth PR, Belot JA, Marks TJ, Chang RPH. 2001. Selective-area atomic layer epitaxy growth of ZnO features on soft lithography-patterned substrates. Appl Phys Lett 79(11):1709–1711.

DOI 10.1002/bit